Available online at www.sciencedirect.com

SCIENCE DIRECT®

Bioelectrochemistry 66 (2005) 9–21

Bioelectrochemistry

www.elsevier.com/locate/bioelechem

Review

Design, synthesis and characterization of monomolecular interfacial layers

G.J. Blanchard[a,*], Paweł Krysiński[b,*]

[a]Michigan State University, Department of Chemistry, East Lansing, MI 48824, USA
[b]University of Warsaw, Department of Chemistry, Laboratory of Electrochemistry, 02-093 Warsaw, Pasteura 1, Poland

Received 20 December 2003; received in revised form 4 May 2004; accepted 14 May 2004
Available online 11 September 2004

Abstract

We have designed a series of monomolecular films comprised of four basic structural motifs. We have used these films for a variety of purposes, ranging from support structures for chromophore arrays to the creation of selective and biomimetic interfaces. We will discuss the several different types of interfacial binding chemistry that are used in the construction of these interfacial films, for both monomeric and polymeric layer structures. Following a discussion of the construction of the adlayers, we describe several uses of these assemblies, in areas ranging from adsorption to optical signal processing, and the formation of biomimetic interfacial structures.

Keywords: Monomolecular films; Chromophore arrays; Biomimetic interfaces

1. Introduction

Surfaces and interfaces are central to processes ranging from cell function to chemical catalysis and sensing. For this reason, there has been a great deal of research effort dedicated to the control and modification of surfaces for predetermined purposes. The surfaces we are interested in are those capable of being used under ambient, atmospheric conditions or in the liquid phase, and significant challenges exist in the design, synthesis and characterization of these systems. We have used a variety of chemical approaches for modification of metallic, semiconductor and insulator interfaces [1–20]. The chemical details of the surface modification depend on the intended application and, for this reason, we have used both ionic and covalent interlayer linking chemistry to construct relatively well-organized interfaces. In this article, we will discuss the chemical means by which individual molecular layers are deposited and bound to one another. Following this discussion, we will outline the use of selected polymers in the formation of multilayer assemblies. Polymers provide lateral interfacial integrity that is not available with α,ω-bifunctional layers. With the design and synthesis of layered interfacial assemblies in hand, we consider several recent uses of these films, including their use in hybrid bilayer systems. We hope that the presentation of these interfacial structural motifs will spark new interest in the design of interfaces for controlling specific properties, such as permeability, and the development of chemically selective and biomimetic interfaces.

One of the key issues in the construction of layered interfaces is the ability to form discrete layers under well-controlled conditions. Among the first examples of multilayer growth was the elegant work of Sagiv showing the formation of layered assemblies using SiO_x chemistry [21–27]. This methodology tends to terminate after several layers of growth due to the use of bifunctional silanes as well as the speed of siloxy bond formation. In parallel with the growth of siloxane multilayers, the alkanethiol/gold monolayer system was discovered and explored [28–37]. Alkanethiol monolayers on gold have proven to be a remarkably versatile system, and multilayer structures have been formed using ω-functionalized alkanethiols in concert with a variety of interlayer bonding schemes. Alkanethiol monolayers serve as a

* Corresponding authors.
E-mail addresses: blanchard@chemistry.msu.edu (G.J. Blanchard), pakrys@chem.uw.edu.pl (P. Krysiński).

1567-5394/$ - see front matter © 2004 Elsevier B.V. All rights reserved.
doi:10.1016/j.bioelechem.2004.05.008

useful interfacial structure when bound to ordered metallic and semiconductor surfaces such as Au, Ag, Cu, Pt and GaAs [38–41], but the attachment of thiols to oxide surfaces such as silica, indium-doped tin oxide (ITO) and alumina or boron-doped diamond (BDD) has not been successful. In order to attach adlayers to this latter family of less well-organized surfaces, different and more robust chemical approaches are required. We will consider here recent progress in the formation of multilayer structures on oxide and other surfaces using ionic and covalent interlayer linking chemistry. We have used these structures to form multilayers using α,ω-bifunctional layer constituents as well as using polymers as layer constituents. We consider several examples that will demonstrate the breadth of interface modification chemistry that is available today. Following an initial discussion of the chemistry used in layer formation, we highlight recent applications of these layered structures.

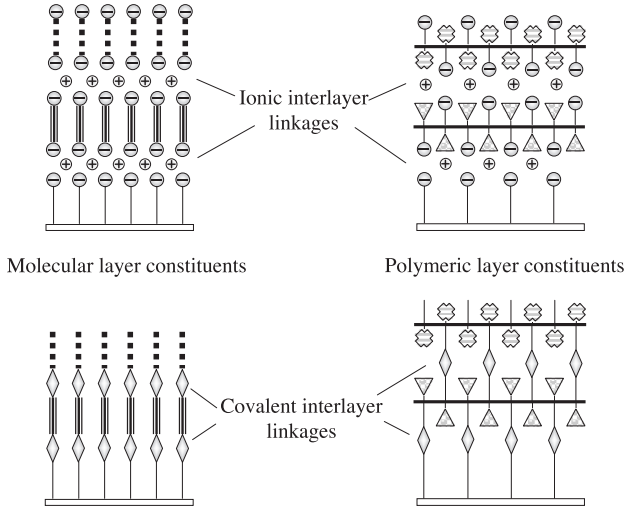

Fig. 1. Schematic depiction of layered growth chemistry, with either monomeric (left) or polymeric (right) layer constituents and ionic (top) or covalent (bottom) interlayer linking chemistry.

2. Structural motifs for layered interfaces

There are essentially four structural configurations that can be used in the construction of layered interfaces (Fig. 1). These are the use of either α,ω-bifunctional layer constituents to form layers characterized by structural integrity normal to the interface plane, or the use of polymers with reactive side groups to form layered sheets with structural integrity both parallel and normal to the substrate plane. Both of these structural motifs can be constructed using either ionic or covalent interlayer linking chemistry. We consider each of these systems in terms of the chemical reactions used to generate the layered structures. For the first two structural motifs discussed, where α,ω-bifunctional adlayer constituents are used, covalent and ionic interlayer linking chemistry may appear to be substantially different, but the same basic principle applies to layer growth in both cases. Each of these growth mechanisms is, at heart, an alternating copolymerization, where for the covalent case the reaction between comonomers involves the formation of a covalent bond, and for ionic layer growth, the comonomers form an ionic complex to create the interlayer attachment.

Ionic bonding of α,ω-bifunctional species is well established in the literature [3,4,42–48]. While there have been a variety of metal ions and anionic functionalities used in the construction of ionically linked multilayers, the system used most widely is zirconium bisphosphonate (ZP) [42–50]. The reason for the dominance of Zr^{4+} or Hf^{4+} lies in the insolubility of these metal phosphonate salts and their fast formation kinetics. The initial step in the preparation of the interface is its modification to contain anionic functionalities capable of binding metal ions. The surfaces most amenable to ionic layer growth are characterized by terminal hydroxyl functionalities (e.g. an ω-hydroxythiol adlayer on Au, SiO_x, ITO), because of the ability of these moieties to interact with $POCl_3$ to form phosphate functionalities. Subsequent growth of layered assemblies requires alternate exposure of the interface to α,ω-bisphosphonates and to metal ions. We note that it is possible to "cap" a surface using this synthetic strategy when both phosphonate functionalities on the α,ω-bisphosphonate react with metal ions in the same layer. This situation can be avoided by using sufficiently high concentrations of the bisphosphonate or by using a rigid bisphosphonate. Because the reaction is so fast for the formation of ZP interlayer linkages, a kinetic product invariably results, as is seen in the IR spectra of layered alkanebisphosphonates, which indicate a liquid-like conformational distribution for the CH_2 groups. Our experimental data suggest that the bond strength for the ZP linkage is in excess of 250 kJ/mol [11], making ZP-bonded multilayers robust materials.

Despite their energetic favorability, the formation of ionic interlayer complexes is not always the ideal means for layer growth. One example is the construction of interfaces where interlayer excitation transport can be controlled. The ZP interlayer "sheets" formed by ionic layer growth are sufficiently polarizable that they serve as a dielectric screen to inhibit interlayer transport [4]. To overcome this limitation, we have developed alternative adlayer growth strategies that involve the formation of less polarizable, covalent interlayer linkages.

There are a variety of synthetic routes available for the formation of covalent interlayer linkages (Fig. 2) and all of them are simple displacement reactions [5,7–9,12,14,15,17–19]. To form covalent adlayers, we can use the same substrates that are used for ionic adlayer growth. We react the surface –OH or $–NH_2$ functionality with the appropriate α,ω-bifunctional molecule, such as a diacid chloride or a diisocyanate, to form a reactive interface. The new reactive

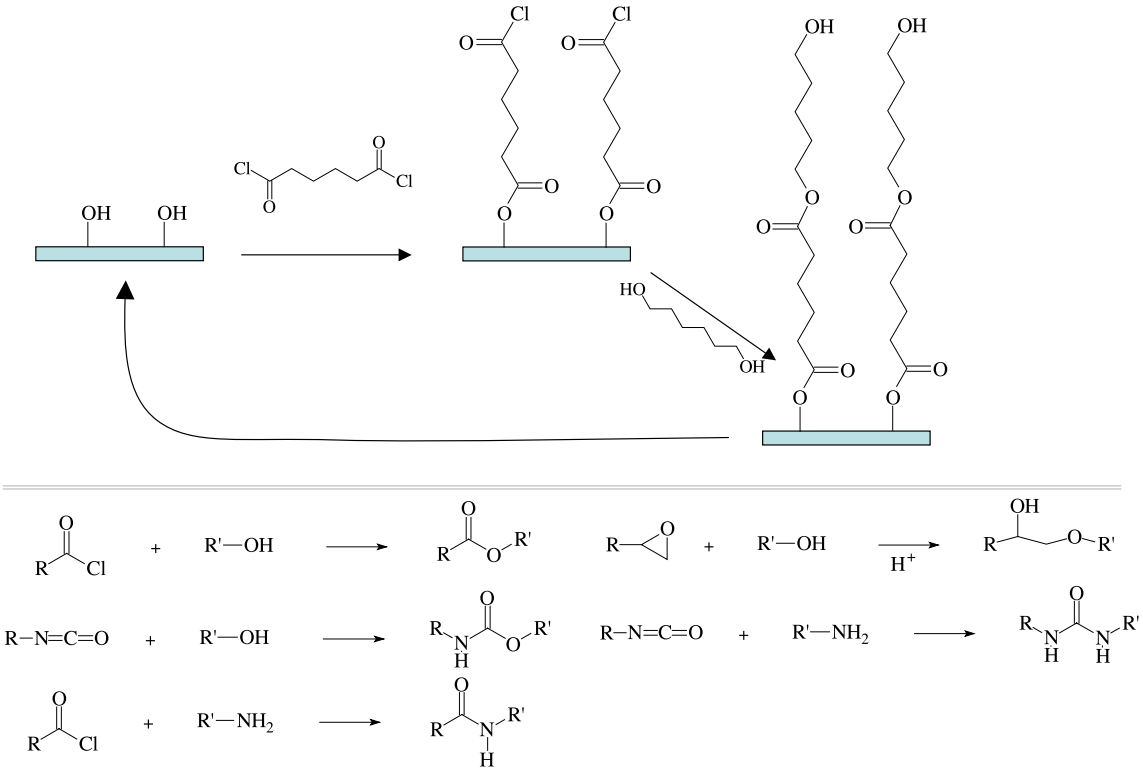

Fig. 2. Top: schematic of covalent multilayer growth using a diacid chloride (adipoyl chloride) and a diol (hexanediol). Bottom: other chemical reactions we have used for the formation of covalently bound multilayer assemblies.

interface is exposed to a complementary α,ω-bifunctional compound such as a diol or diamine, to form the subsequent layer, and the sequence of exposing the resulting interface to its reactive complement can be continued. The initial demonstration of this type of covalent adlayer growth was made using diamines and diisocyanates to form urea interlayer linkages, with both of the comonomers being sufficiently rigid that self-termination did not play a significant role in limiting interface reactivity [7]. We have subsequently demonstrated the formation of multilayers using diols or diamines with diacid chlorides to form ester or amide linkages, respectively, as well as several other reactions [15].

These reactions and methodology for adlayer growth can be applied to the formation of polymeric multilayers, where the overall interfacial assembly is best described as a layer-by-layer cross-linked polymer network [7,8,14,15]. Our approach to the formation of polymer multilayers is to synthesize the polymers with side groups that are appropriate for either the ionic or covalent interlayer linking chemistry discussed above. The polymer we use for this work is a maleimide-vinyl ether (MVE) alternating copolymer (Fig. 3) [51]. We have chosen this family of polymers for several reasons: (1) MVE polymers are structurally regular, allowing for the incorporation of known amounts and types of side groups at well-defined intervals along the polymer backbone; (2) MVE polymers are synthesized readily and there is substantial freedom in the choice of side groups of the maleimide and vinyl ether monomers; and (3) these materials are structurally robust; once the polymer adlayers are formed, they are not susceptible to chemical or thermal degradation under ambient conditions.

Using MVE polymers, we have demonstrated regular multilayer growth using both ionic and covalent interlayer linking strategies (Fig. 3) [5,7–9,14,15]. For ionic interlayer bonding, we must use bromotrimethylsilane partial deprotection chemistry of protected phosphonate side groups to allow for multilayer growth [52]. Once the polymer is bound to the surface, the remaining isopropylphosphonate groups are deprotected and subsequently zirconated so that they can be used to bond to a subsequent adlayer [5]. For a given polymer adlayer within the assembled interface, there is no guarantee that 50% of the polymer phosphonate side groups bind to their underlayer and 50% are used to bind to an overlayer, and this is an issue that will depend on the details of the selective deprotection chemistry. The fact that there are available deprotected phosphonates available for each interlayer binding step ensures the facile formation of the layered assembly.

For covalent polymer layer bonding, there is not the corresponding need for selective deprotection because of the nature of the chemistry used. We have demonstrated facile multilayer growth using MVE polymers with covalent interlayer linking chemistry and without the need to resort to selective protection/deprotection schemes [15]. The resulting multilayers show regular growth, both in terms of layer thickness and absorbance, and we have seen no loss of reactivity with the addition of layers.

3. Utility of adlayer structures

Using the several layered interface growth strategies outlined above, we now consider selected applications and the characterization of a representative sampling of these systems. Our interest in layered interfaces ranges from optical information storage to chemical separations and the development of biosensors, and we will consider each of these areas separately.

3.1. Excitation transport to characterize interface morphology

We have used ZP-linked multilayers comprised of α,ω-bifunctional species to understand the surface morphology of silica [3]. Silica is a widely used interface for chemical separations and the density of surface silanol groups can be controlled to a limited extent. On the molecular scale, however, it is not clear how the surface silanol groups are distributed. To evaluate interface morphology, we have performed excitation transport experiments on ZP monolayers bound directly to silanol groups. The monolayers we use for this work were made with varying concentrations of bisphosphonated oligothiophene chromophores, where bithiophene (BDP) functions as an optical donor and quaterthiophene (QDP) acts as an optical acceptor. These layers exhibit chromophore population decay dynamics that can be understood in the context of an excitation hopping model [53], but are inconsistent with the standard presentation of the Förster model [54]. From the excitation hopping model, we can extract the size of the islands sensed spectroscopically and compare this information to the physical dimensions we recover from AFM measurements [3]. The correspondence between the two measures of island size reflects the relationship between spectroscopic and physical domains, and for these interfaces, the two domain sizes are in remarkably good agreement.

We construct three-component monolayers using BDP, QDP and an optically inert bisphosphonate. The fractional amount of each species present in the adlayer can be controlled through the solution phase concentration ratios of the bisphosphonates in the deposition solution [3]. The time-domain spectroscopic characterization of these monolayer assemblies shows that the optical donor population decays approximately as a two-component exponential, and neither the time constants nor the prefactors of the exponential components depend on BDP concentration. This apparently anomalous behavior is a consequence of the morphology of the adlayer. For a spatially heterogeneous system, we consider the chromophores (donor or acceptor) to be present in the form of aggregated islands, with a minor fraction of the chromophore present in non-aggregated regions (Fig. 4). For such a system, the aggregates will absorb most of the light based simply on the preponderance of absorbing species being present in that form [53]. The chromophores contained in the aggregates are assumed in this model not to emit light efficiently; the chromophores that dominate the radiative response are not coupled to the aggregates, and their proximity to the aggregates is related to their lifetime. This latter assumption is made based on the putative dielectric gradient in which these (radiative) chromophores reside. In principle, we should detect a continuous distribution of

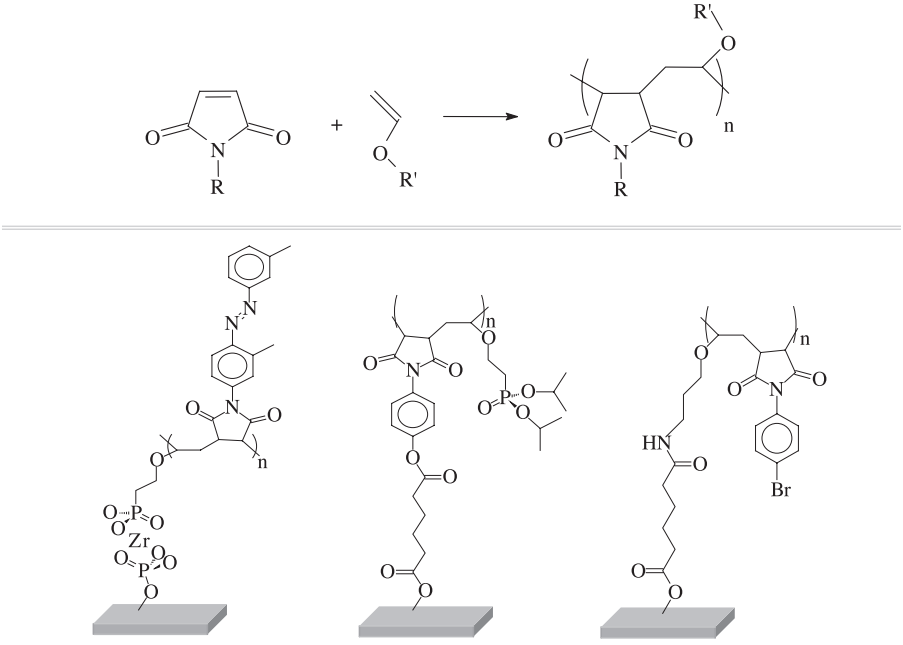

Fig. 3. Top: schematic of synthesis of maleimide-vinyl ether alternating copolymer. Bottom: schematic indicating different methodologies for deposition of polymer adlayers. Polymers can be bonded to substrates or other polymer layers through their vinyl ether side groups using ZP chemistry (left), and either through the maleimide (center) or the vinyl ether (right) side groups using covalent linking chemistry.

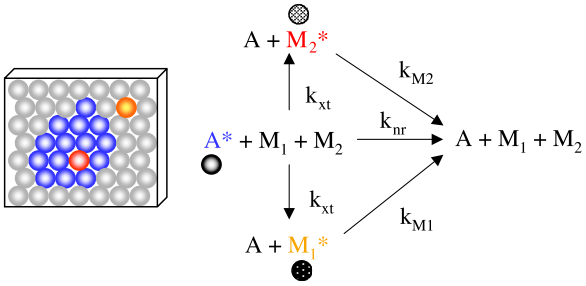

$$\frac{d[A^*]}{dt} = -k_{xt}[A^*]([M_1]+[M_2]) - k_{nr}[A^*]$$

$$\frac{d[M_1^*]}{dt} = -k_{M1}[M_1^*] + k_{xt}[A^*][M_1]$$

$$\frac{d[M_2^*]}{dt} = -k_{M2}[M_2^*] + k_{xt}[A^*][M_2]$$

$$\frac{d[M_1]}{dt} = k_{M1}[M_1^*] + k_{xt}[A^*][M_1]$$

$$\frac{d[M_2]}{dt} = k_{M2}[M_2^*] - k_{xt}[A^*][M_2]$$

Fig. 4. Top: cartoon and excitation relaxation pathways of aggregated surface, with radiative monomers (red and orange) in different spatial proximities to aggregated (blue) species. Bottom: the series of coupled differential equations that describe the relaxation process.

lifetimes based on the proximity of the radiative chromophore(s) to nearby aggregates, but the signal-to-noise ratio of our experimental data limits our ability to discern more than two decay components. The functionality and concentration-independence of the donor emission response are indicative of a spatially heterogeneous adlayer structure. The most instructive feature of the radiative response of the adlayer donors is the build-up in emission response subsequent to excitation (Fig. 5). These data show that there is a measurable increase in signal intensity following the peak of the instrument response function, corresponding to random-walk excitation transport on the aggregate prior to its migration to a radiative chromophore [53]. Because the time resolution of our time correlated single photon counting system is ~35 ps, and we are limited in our ability to deconvolute the response from the data for S/N reasons, we can only determine that the time constant of the build-up is 10 ps or less. This upper limit on the build-up time corresponds to an aggregate island size of 50–100 Å in diameter, depending on the excitation hopping rate and the shape of the island. AFM data on these same interfaces [3] reveal a physical topology in excellent agreement with our spectroscopic findings, suggesting that the characteristic spectroscopic domain size we sense is limited by the physical dimension of the island structure on these surfaces.

It is important to consider the origin of the spatial heterogeneity we find in SiO_x-bound adlayers. There are several ways to attach ZP monolayers to silica surfaces. Substrate priming with aminopropyltriethoxysilane (APTES) yields ~30 Å surface coverage, indicating substantial primer polymerization. This polymerization can be eliminated by either of two methods; reaction of the SiO_x surface with aminopropyldimethylmethoxysilane (APDMES) or by direct reaction of surface silanol groups with $POCl_3$. Both of these priming methods produce monolayer coverage of the silica surface without unwanted polymerization. We obtain the same spectroscopic results for the formation of optical donor/acceptor monolayers using any of these initial surface reactions, indicating that the spatial heterogeneity we detect is intrinsic to the silica substrate and is not a consequence of our reaction chemistry. This finding has significant implications for chromatographic separations and opens the door to the use of polymeric adlayers to alter the density and distribution of chemically reactive functional groups present at the substrate surface.

3.2. Biomimetic interfaces bound to electrode surfaces

We have used covalent interfacial bonding chemistry as a facile means of constructing a hybrid bilayer assembly [55]. We are interested in creating interfaces that are characterized by the presence of both hydrophilic regions and hydrophobic regions that lie in spatially well-defined layers

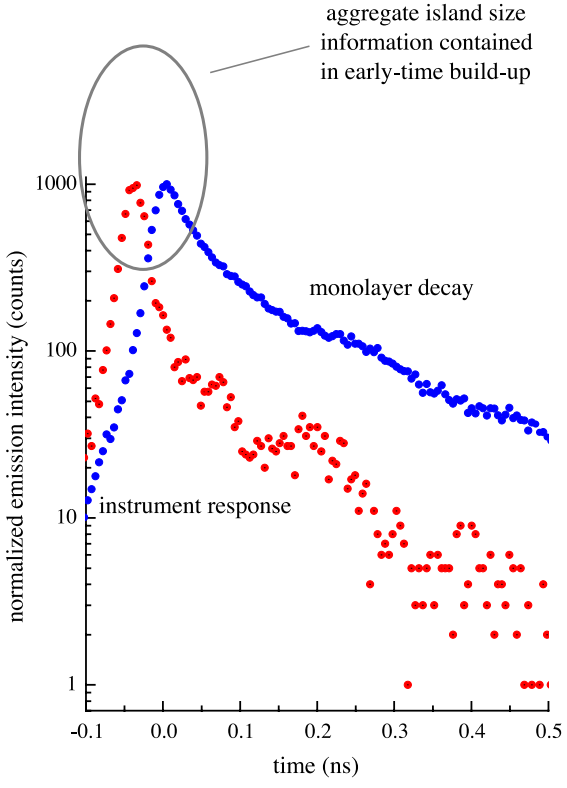

Fig. 5. Time-correlated single photon counting data showing the instrument response function and the relaxation dynamics of surface bound BDP. The build-up time following the maximum of the instrument response function results from excitation migration on the aggregate islands. Deconvolution shows the build-up time to be ≤10 ps.

parallel to the substrate surface. This structural motif is useful for biomimetic sensors, where the hybrid bilayer assembly can function as a lipid-like medium to support transmembrane proteins in their active conformation in a location amenable to electrochemical signal transduction. An interfacial structure characterized by a hydrophilic region adjacent to the substrate is, in general, not readily accessible with alkanethiol or alkylsilane layer growth chemistry. The chemistry we utilize relies on the reaction of a substrate interfacial oxide with an acid chloride such as adipoyl chloride or tetradecanoyl chloride to form an ester-like bond. For an ITO-coated substrate, the interfacial oxide is a native indium doped tin oxide deposited on quartz and for the gold substrate the interfacial oxide layer is generated electrochemically. For both ITO and Au substrates, after the initial deposition of adipoyl chloride, the resulting terminal acid chloride functionality is reacted with *n*-dodecylamine to produce an interfacial monolayer of n-dodecyladipamide (designated C_6–A–C_{12}, Fig. 6). We compare the behavior of the C_6–A–C_{12} interface to that of a monolayer formed from tetradecanoyl chloride (designated C_{14}, Fig. 6). Our primary interest at this point lies in characterizing the structure and properties of the C_6–A–C_{12} and C_{14} interfaces, and how these systems respond to the physisorption of a lipid adlayer (Fig. 6).

The C_6–A–C_{12} and C_{14} interfacial structures are characterized by a hydrophilic region in close proximity to the electrode surface, with hydrophobic structure beyond the hydrophilic region [56]. For C_6–A–C_{12}, there is a second hydrophilic region comprised of amide bonds, spaced apart from the first hydrophilic region. Both the oxide substrates and the adlayers lie within our structural control synthetically, and the thickness and spacing of hydrophilic and hydrophobic regions can be adjusted to create interfaces that can serve as substrates or initial layers in hybrid bilayer membranes (HBMs) [57,58]. The incorporation of hydrophilic and hydrophobic regions in an adlayer at well-defined distances from the substrate can be superior to other methods for supporting biomolecules at interfaces. Amide- and ester-containing adlayer structures can form hydrogen bonded networks parallel to the substrate plane that can interact strongly with adsorbed species and can support an ionic reservoir between the hydrophobic portion of the adlayer and the substrate surface.

Our goal in designing amphiphilic interfaces is ultimately to incorporate selected proteins into the interfacial adlayer while retaining their biofunction. For this purpose, we have constructed biomimetic hybrid bilayers where the substrate-bound side of the adlayer will be fluid-like. Clearly, such a system will be less fluid than a true lipid bilayer structure and, for these systems, the manifestation of fluid-like behavior will depend on the manner in which the system is examined. IR data indicate a fluid-like environment based on band position and linewidth of the CH stretching resonances, and time-domain fluorescence data of chromophores imbedded in

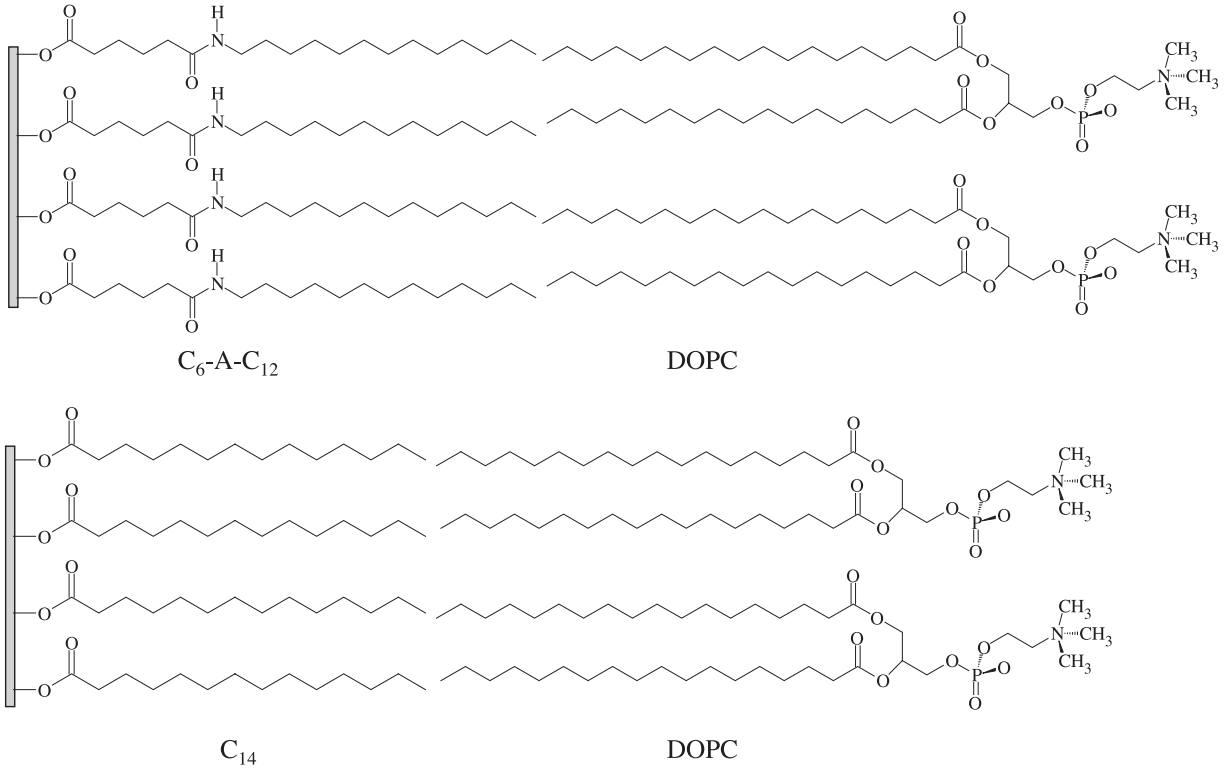

Fig. 6. Schematic depiction of hybrid bilayer assemblies. These cartoons are not intended to imply specific registration of the physisorbed layer with the covalently bound layer. Top: a C_6–A–C_{12} layer covalently bound to a substrate, capped with a physisorbed layer of DOPC. Bottom: a C_{14} layer covalently bound to a substrate, capped with a physisorbed layer of DOPC.

the interface reveal an environment that is substantially rigid on a ~20-ns timescale. Only when these interfaces are examined from a variety of standpoints, both spectroscopic and electrochemical, does a true picture of their properties emerge.

Infrared reflectance–absorbance spectra can provide steady state orientational and conformational information on the hydrocarbon chains in the C_6–A–C_{12} (25 Å ellipsometric thickness) and C_{14} (18 Å ellipsometric thickness) SAMs, when they are grown on reflective substrates. Well-ordered, densely packed alkyl chains in *n*-alkanethiol SAMs on gold have $CH_{2(as)}$ and $CH_{2(sym)}$ bands at 2918 and 2850 cm^{-1}, respectively, being shifted by 5–9 cm^{-1} to the red relative to the spectral features seen for disordered monolayers [33,59]. The relative intensities of the methylene stretches have been used to obtain quantitative information about alkyl chain orientation for *n*-alkanethiols on several coinage metals [33,59–62]. While our systems are not the same as alkanethiols on gold, the principles of the measurement and qualitative interpretation of the data remain largely the same. Typical IR reflection–absorption spectra have features between 2700 and 3100 cm^{-1} for the C_6 adlayer, the C_{14} adlayer and the C_6–A–C_{12} layer on oxidized gold substrates (Fig. 7). The CH stretching vibrations of the C_6 and C_6–A–C_{12} adlayers are most similar to those of liquid-like films. The relative intensities of asymmetric $–CH_2–$ and $–CH_3$ stretches suggest some ordering in the C_{14} and C_6–A–C_{12} adlayers, consistent with earlier work on DPPE-mercaptopropionamide monolayers on gold [63].

We can gain additional insight into the nature of the adlayer bonding to the surface by taking advantage of the fact that ITO is a semiconductor. We apply a Mott-Schottky analysis to our data to detect changes in the flatband potential, U_{fb}, of the ITO semiconductor electrode. This effect has been reported for ITO and silanized ITO surfaces [64–66]. We measured the dependence of the space charge capacitance, C_{sc}, on the applied potential for bare ITO electrodes and ITO with C_{14} and C_6–A–C_{12} adlayers bound covalently. We acquire C_{sc} directly from complex AC voltammetry data. The analysis of impedance data in terms of appropriate equivalent circuits leads to capacitance and resistance values of the circuit elements used, allowing the separation of space charge and monolayer capacitances. In the low frequency regime, the change in the overall impedance of the ITO/monolayer interface is not correlated with the adlayer impedance, but is attributed to the decrease of the space charge capacitance, C_{sc} [64–66]. We observe a capacitance drop from 41 μF/cm^2 for the bare ITO surface to 10 μF/cm^2 for adlayer-coated ITO. By comparison, a well-ordered alkanethiol monolayer yields a value for C_{sc} of 1.14 μF/cm^2 [67]. We assume the monolayer capacitance is constant over the potential range we access, so the dependence of the interfacial capacitance on applied potential is dominated by C_{sc}. We extract a flatband potential value of U_{fb}=−0.58 V for bare ITO, in agreement with other reports

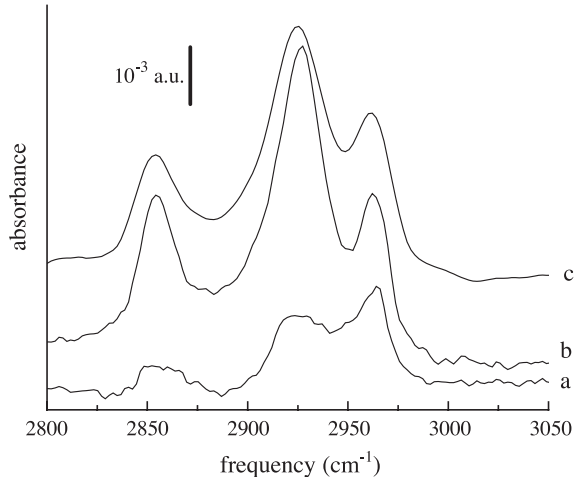

Fig. 7. FTIR spectra taken with 4 cm^{-1} resolution of the CH stretching region of (a) an adipoyl chloride adlayer, (b) a C_{14} adlayer and (c) a C_6–A–C_{12} adlayer. The spectra have been offset for clarity.

[65]. The addition of either C_{14} (U_{fb}=−0.51 V) or C_6–A–C_{12} (U_{fb}=−0.50 V) adlayers shifts U_{fb} positive by 70–80 mV, indicating the surface state distribution has been modified by the covalent attachment of the adlayers to the surface hydroxyl groups. A positive shift of similar magnitude has been seen for alkylsiloxane monolayers bound to ITO [65].

The capacitance of the interface between a metallic (Au) electrode and the solution is a characteristic of the adlayer density and organization. We cannot use capacitance to characterize the adlayer bound to the ITO electrode because of contributions from space charge capacitance, C_{sc}. For the Au electrode, a well-organized adlayer should be substantially impermeable to electrolyte, resulting in a small monomolecular adlayer capacitance, C_m, that is related to the adlayer thickness, d, by the parallel plate capacitance equation,

$$C_m = \frac{\varepsilon\varepsilon_0 A}{d} \quad (2)$$

A is the electrode area, ε_o is the dielectric constant of the vacuum and ε is the apparent dielectric constant of the adlayer. If the adlayer contains defects, such as disordered chains or pinholes, electrolyte will penetrate the film, yielding a capacitance value larger than predicted by the model [61,68–70]. The capacitance characteristics of C_6–A–C_{12} and C_{14} adlayers on gold are derived from complex AC voltammetric measurements (Fig. 8). We have also physisorbed a DOPC overlayer onto the C_6–A–C_{12} and C_{14} adlayer structures. Because of the apparent parabolic dependence of the capacitance as a function of potential for both C_6–A–C_{12} and C_{14} adlayers, we believe there to be potential-dependent changes in aliphatic chain organization and/or electrostriction within these structures [70–75]. For the C_6–A–C_{12} adlayer, C_m=1.22 μF/cm^2 corresponds closely to the value expected for a defect-free monolayer of densely packed alkanethiols of comparable

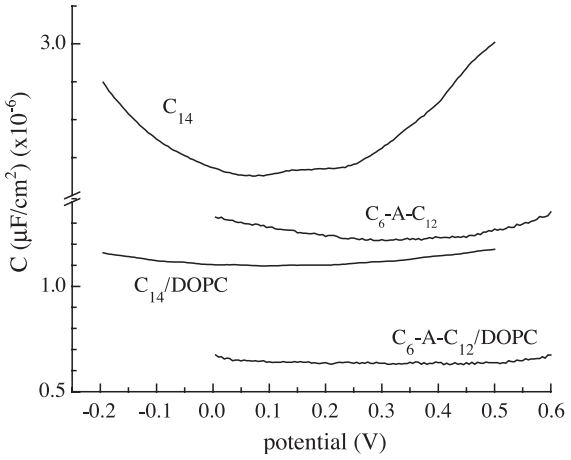

Fig. 8. Capacitance as a function of potential for HBM adlayer structures, indicated next to each curve.

length [67]. The C_{14} adlayer exhibits C_m=2.66 μF/cm^2, implying higher permeability than for the C_6–A–C_{12} adlayer. We attribute this difference to the presence of a hydrogen-bonded network within the adlayer which serves to isolate the surface from the bulk.

The quality of the adlayer bound directly to the substrate is also reflected in the behavior of HBMs formed on their surfaces. We obtain C_{HBM}=0.65 μF/cm^2 from the capacitance/voltage curve of the C_6–A–C_{12}/DOPC HBM, a value fully consistent with the 0.5–1 μF/cm^2 range that has been seen for bilayers tethered to gold using hydrophilic spacers [76–78]. By comparison, the capacitance of a solvent-free lipid bilayer membrane is C_{BLM}=0.8 μF/cm^2 [79]. We can model the hybrid bilayer structure in the context of a pair of capacitors in series. We recover C_{DOPC}=1.6 μF/cm^2, in agreement with the value of a DOPC monolayer densely packed on mercury, and with other HBMs [63,80,81].

The presence or absence of defects and pinholes in our HBM and adlayer structures can be examined using cyclic voltammetry and ac voltammetry. Systematic analysis of cyclic voltammograms (CV) often allows for the differentiation among possible mechanisms of electron transfer at monolayer-modified electrodes [61,68,82]. For well-ordered, defect-free films, CV exhibits a nearly exponential current–potential dependence, indicating through-chain electron transfer. Spherical diffusion-limited electron transfer, characteristic of pinholes, produces a sigmoidal CV curve. The CVs of C_6–A–C_{12}/DOPC and C_{14}/DOPC hybrid bilayers on gold and ITO show that, even though the Faradaic current is almost two orders of magnitude smaller than that for bare electrodes, there is a significant contribution from radial-diffusion limited electron transfer of the K_4 [Fe(CN)$_6$] redox probe. This same behavior is more pronounced for the C_6–A–C_{12} and C_{14} adlayers alone, suggesting the presence of widely spaced pinhole defects (>5 Å radius) to allow direct electron transfer between the redox probe and the electrode surface [61,68,83]. Such defects are most likely a consequence of the relatively short adlayer constituents we use. Discontinuities in the surface gold oxide layer [84] can produce point defects and grain boundaries that would be unaffected by the covalent adlayer bonding chemistry we use. Regardless of the exact origin of the defects, the addition of a DOPC overlayer seals them significantly, creating a relatively well-ordered hybrid bilayer membrane where the underlayer is bound covalently to the substrate.

Polymeric adlayers have proven to be of great use in probing and controlling selected interfacial properties. We have examined both ionically and covalently bound polymeric multilayer structures and from these studies we have gained insight into the strength of interlayer linking chemistry that holds these structures together, as well as understanding the potential for this family of materials to function as chemically selective structures. We consider these areas separately.

3.3. Polymer side group isomerization as a means of gauging interlayer bonding strength

In an effort to understand the structural freedom of polymeric multilayers and at the same time to evaluate the relative strength of the chemical and physical forces responsible for the formation of polymeric ZP multilayers, we have undertaken a study using maleimide-vinyl ether alternating copolymers with isomerizable side groups. We have grown layered assemblies of poly(4-*N*-maleimidoazobenzene-*c*-(2-vinyloxy)-ethylphosphonate) (poly(MAB-VEP)), where interlayer connections are made using zirconium-bisphosphonate (ZP) ionic complexation chemistry [11]. The absorption spectroscopy of the azobenzene side groups shows constant layer density but a layer-dependent ratio of *trans*-to-*cis* isomers. Ellipsometric thickness data show a constant average layer thickness despite the change in *cis*-to-*trans* side group conformer ratio. The layer-dependent conformational changes result from the steric constraints imposed on the polymer side groups by the formation of the ZP interlayer linkage(s). Once the layers are formed, the side-groups do not have sufficient structural freedom to back-convert to the *trans* conformer, even when exposed to UV for a prolonged period.

We have grown up to seven layers of poly(MAB-VEP). Poly(MAB-VEP) exhibits a constant average layer thickness of 21.7 Å/layer. Absorption spectroscopic data reveal the steric restrictions placed on the azobenzene side groups by the formation of the interlayer ZP linkages. We show in Fig. 9 the absorbance spectra of the poly(MAB-VEP)-modified interface as a function of number of layers added. These spectra are dominated by the absorbance of the azobenzene side groups in the 230–400 nm region. We determine the density of chromophores from the absorbance data using the *trans* (ε_{313}=25,000 M^{-1} cm^{-1}) and *cis* (ε_{250}=13,000 M^{-1} cm^{-1}) conformer extinction coefficients

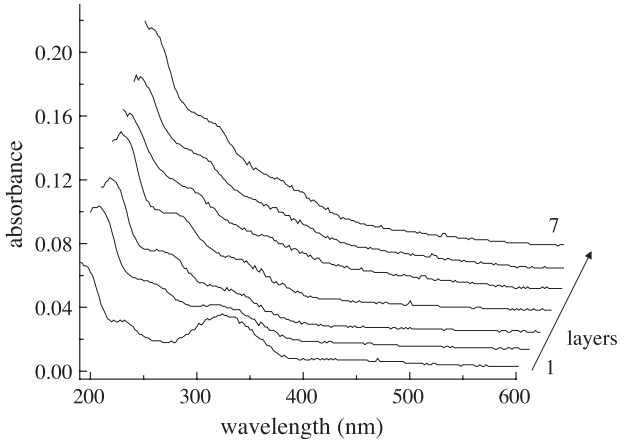

Fig. 9. Absorbance of poly(MAB-VEP) layers as a function of layer deposition, shown offset for clarity. The band positions for the first layer (bottom) are shifted from those for layers 2–7 and the band intensity ratios vary with number of adlayers.

[85–87]. The absorbance data indicate a constant amount of polymer is being deposited for each layer. The bands for the first layer appear to be shifted relative to those for subsequent layers, as a result of the gradient in the dielectric response of the system over the length scale of the chromophore [88–92] for the first polymer adlayer. Perhaps, most significant is the observation that the ratio of the azobenzene side group *trans* (313 nm) and *cis* (250 nm) bands depends sensitively on the number of polymer layers. The fact that the conformer ratio changes with the number of polymer layers means that the azobenzene side groups are confined significantly by their local environment and the driving force for the formation of the multilayer assembly must exceed the energetic cost associated with isomerization of the ground state chromophore. This situation is true even for the first layer, where [*trans*]/[*cis*]=0.59.

In contrast to our polymer layer data, solution phase azobenzene exhibits essentially no *cis* conformer. Our finding that only 60% of the side groups are *trans* in the first polymer layer underscores the steric limitations imposed on the polymer side group by the ZP layer linking chemistry. For the spin-cast film, we recover a predominantly *trans* conformation since there is no opportunity for sterically restrictive bond formation to occur within the spin-cast matrix. The ground state barrier for the isomerization of azobenzene is thought to be on the order of 105 kJ/mol [93]. We estimate the strength of RPO_3–Zr–O_3PR group formation based on the limited information available in the literature on the solubility of zirconium phosphates. We take with some trepidation the value of $K_{sp}=10^{-132}$ for $Zr_3(PO_4)_4$ [94],

$$Zr_3(PO_4)_4 \overset{K_{sp}}{\rightleftharpoons} 3\ Zr^{+4} + 4\ PO_4^{-3}$$

If we assume this value is correct and apply it to the formation of RPO_3–Zr–O_3PR, where the metal to ligand ratio is different, we can estimate the equilibrium constant for RPO_3–Zr–O_3PR formation based on the concentration of free Zr^{4+}. We infer $K_{eq}=10^{44}$ for the reaction

$$Zr^{4+}+2RPO_3^{-2} \rightleftharpoons Zr(RPO_3)_2$$

and from this estimate, we calculate $\Delta G=-250$ kJ/mol. In principle, the ZP complexation process could be mediated by the photoinduced isomerization behavior of the side groups. It is possible that ZP complex formation proceeds only when ambient light "toggles" a side group to the *cis* conformation and the complex cannot form if the side group remains *trans*. To evaluate this possibility, we deposited poly(MAB-VEP) multilayers in the dark, precluding photoisomerization of the azobenzene side groups. Ellipsometric data (632.8 nm) show no light-dependence on the formation and thickness of adlayers, suggesting room light is not a mediator in the adlayer deposition process.

It is useful to consider the values of the [*trans*]/[*cis*] ratio and how they correspond to fractional concentrations of each isomer. For the first layer, where [*trans*]/[*cis*]=0.59, the surface is comprised of 63% *cis* isomers and 37% *trans* isomers. Even for the first layer, there is considerable steric restriction placed on the azobenzene side group and this finding suggests a significant role of surface topology in determining first layer morphology. For the second layer, [*trans*]/[*cis*]=0.43, or 70% *cis* and 30% *trans* overall. Since the loading density is constant for each layer, it is tempting to speculate that the second layer is 77% *cis* and 23% *trans*. This ratio holds relatively constant for subsequent layers. Because of the nature of the measurement, we cannot extract the layer-by-layer fractional concentrations of *cis* and *trans* isomers. The fact that the *trans* absorbance decreases with the addition of a second layer demonstrates that we cannot treat these interfaces as isolated layers.

Once the polymer adlayers are formed, interconversion between side group isomers is not facile. The driving force for interlayer bonding prevents back-isomerization. We have irradiated a four-layer poly(MAB-VEP) assembly with a Hg lamp (254 nm) for several hours. We irradiated the $S_2 \leftarrow S_0$ transition for the *cis* side group conformer at 254 nm to convert the existing *cis* conformers in the polymer assembly into the more stable *trans* conformer. We observed no change in the spectral profile of the four-layer assembly, nor any change in the ellipsometric thickness as a result of UV irradiation. Once the adlayers are bound to the interface, the azobenzene conformers are effectively locked and the steric restriction imposed by the layered polymer matrix is sufficient to prevent isomerization of the polymer side groups. It is likely that greater structural freedom can be designed into the polymer adlayer structures, leading to more facile side group isomerization, but we have not investigated this issue in detail to date.

3.4. Using polymer multilayers to impart chemical selectivity to interfaces

We have also used polymeric multilayer assemblies to mediate the adsorption and desorption kinetics of interfaces, with an eye toward controlling chemical selectivity at these interfaces. We deposit maleimide-vinyl ether alternating copolymer layers, where each polymer layer contains different pendant side group functionalities, and the order of layer deposition is controlled. The adsorption isotherm behavior of these interfacial structures, when exposed to methanol and hexane vapor, shows that the identity of the adsorbates and the order of polymer adlayer deposition both influence the interfacial adsorption characteristics. The absence of hysteresis in the isotherm data show our measurements to be made under equilibrium conditions, implying chemical and structural control over the thermodynamics of adsorption.

We measure the gas–solid adsorption isotherms for these bilayer structures using quartz crystal microbalance (QCM) gravimetry. For a QCM, there is a linear relationship between mass uptake and frequency shift, as described by the Sauerbrey equation [95],

$$\Delta f = \frac{-2\Delta m (f_0)^2 n}{A(\mu\rho)^{1/2}} \tag{3}$$

In Eq. (3), Δf is the change in frequency of the QCM associated with a mass increase, Δm is the mass change, f_0 is the QCM oscillation frequency (~6 MHz), n is the harmonic of the fundamental frequency (n=1 in these measurements), A is the exposed area of the QCM, and μ and ρ are the shear modulus (2.947×10^{11} g cm^{-1} s^{-1}) and density of quartz (2.648 g cm^{-3}), respectively.

The form of the adsorption isotherms we measure for these polymer adlayer stacks is related to the energetics of adsorption and the interface morphology. We use the BET model [96] to treat our data because of its versatility and demonstrated applicability to interfacial adsorption phenomena [97]. We recognize that the BET model will not fit all of our data over the entire adsorbate partial pressure range, but for limited adsorbate concentration ranges, this model can be used to extract useful information. The BET isotherm relates the volume of adsorbate (assuming bulk density) to its partial pressure in the vapor phase [97],

$$V_{\text{ads}} = \frac{V_{\text{ml}} c z}{(1-z)\{1-(1-c)z\}} \tag{4}$$

V_{ads} is the volume of the adsorbate, V_{ml} is the volume of the monolayer and z is the fractional vapor pressure, normalized to the saturation vapor pressure, $z=p/p^*$. The term c is related to the relevant energies of interaction (ΔH_{des}=enthalpy of desorption of the adsorbate from the surface, ΔH_{vap}=enthalpy of vaporization of the bulk adsorbate).

$$c = \exp\left(\frac{\left(\Delta H_{\text{des}} - \Delta H_{\text{vap}}\right)}{RT}\right) \tag{5}$$

We use ΔH terms on the assumption that $\Delta S_{\text{des}}=\Delta S_{\text{vap}}$. Depending on the adsorbate and polymer adlayer used, we have found that the dominant interaction between the adsorbate and the interface occurring at the metallic or modified dielectric surface, beneath the polymer adlayer [16]. The functional form of the adsorption isotherm depends on the polymer and adsorbate identities and order of polymer adlayer deposition. For low adsorbate partial pressures, z, the data can be modeled using the BET adsorption isotherm and for higher z, the BET model tends to overestimate adsorption. We limit the fitting of our data to the adsorbate partial pressure range $0\leq z\leq 0.4$ to remain in a region where the application of the BET isotherm is clearly appropriate. We use methanol and n-hexane as adsorbates, and our data demonstrate substantial solvent and adlayer-order dependencies in the isotherms (Fig. 10). From the ΔH_{des} values extracted from fits of the data to the BET isotherm, we find $K=k_a/k_d$ for each system (Table 1),

$$\ln\left(\frac{k_a}{k_d}\right) = \frac{\Delta H_{\text{des}}}{RT} - \frac{\Delta S_{\text{vap}}}{R} \tag{6}$$

The values of K and the functionality of the adsorption isotherm varies substantially between different adlayer/adsorbate combinations, and this finding shows clearly that we have established control over chemical selectivity using

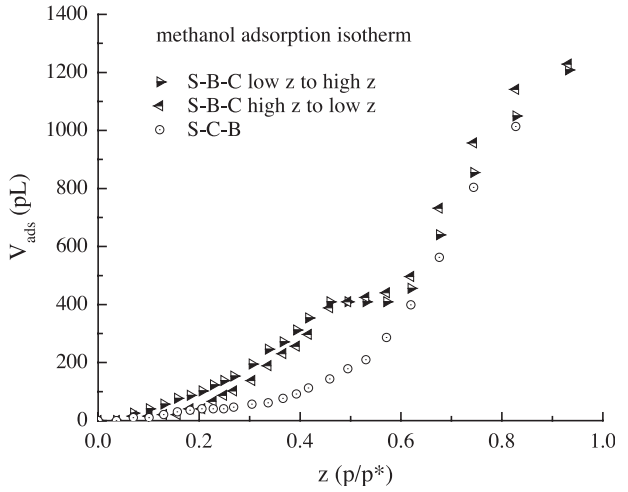

Fig. 10. Adsorption isotherm data for interaction of vapor phase methanol with two substrate-bound polymer bilayers: (○) S–C–B=substrate–poly(3-chlorophynylmaleimide-aminopropylvinyl ether)–poly(4-bromophenylmaleimide-aminopropylvinyl ether), data taken from low z to high z. (➢) S–B–C=substrate–poly(4-bromophenylmaleimide-aminopropylvinyl ether)–poly(3-chlorophynylmaleimide-aminopropylvinyl ether), data taken from low z to high z. (◅) S–B–C=substrate–poly(4-bromophenylmaleimide-aminopropylvinyl ether)–poly(3-chlorophynylmaleimide-aminopropylvinyl ether), data taken from high z to low z, indicating the absence of hysteresis.

Table 1
Values of $K=k_a/k_d$, calculated using Eq. (6)

Interface	$K=(k_a/k_d)$ (methanol)	$K=(k_a/k_d)$ (hexane)
S-BPM-NPM	31.25 (+8.75, −5.61)	47.6 (+14.9, −9.1)
S-NPM-BPM	2.42 (+0.34, −0.27)	3.70 (+0.61, −0.39)
S-BPM-CPM	0.53 (+0.13, −0.09)	5.38 (+1.16, −0.81)
S-CPM-BPM	5.56 (+2.77, −1.39)	0.40 (+0.05, −0.05)
S-BPM-HPM	3.45 (+0.72, −0.51)	–
S-HPM-BPM	385 (+70, −52)	–
S-HPM[a]	2.94 (+0.29, −0.24)	–
S-BPM[a]	4.55 (+2.59, −1.22)	–
S-CPM[a]	2.86 (+0.17, −0.16)	–

For these calculations, ΔH_{vap}=37.43 kJ/mol and ΔS_{vap}=111 J/mol K for methanol, ΔH_{vap}=31.56 kJ/mol and ΔS_{vap}=92 J/mol K for hexane. Abbreviations for the interfaces are as follows: S=substrate, BPM=poly(4-bromophenylmaleimide-aminopropylvinyl ether), CPM=poly(3-chlorophynylmaleimide-aminopropylvinyl ether), NPM=poly(*N*-phenylmaleimide-4-hydroxybutylvinyl ether) and HPM=poly(4-hydroxyphenylmaleimide-vinyl ether ethylphosphonate). In all cases, adipoyl chloride is used as the interlayer linking moiety.

[a] Values extracted from data in Ref. [16].

polymer adlayers that are tens of Å thick. One may infer from our findings that the control we exert is thermodynamic control, but this issue remains to be established. The achievement of thermodynamic control could be demonstrated only if the data acquired at each point along the adsorption isotherms are at thermodynamic equilibrium. We test for this condition by acquiring experimental data for both increasing and decreasing z. If the data acquired under both conditions are the same to within the experimental uncertainty (Fig. 10), we are either operating at thermodynamic equilibrium or we have achieved a different steady state condition for each value of z. We assert that the latter situation is not physically reasonable.

4. Conclusions

We have discussed several structural motifs for layered interfacial assemblies that have been demonstrated and used for selected applications in our laboratories. We can bind either monomolecular species or polymers to interfaces one layer at a time using either ionic or covalent interlayer linking chemistry. Using these several structures, we have described their use in areas ranging from characterizing the distribution of chemically reactive sites on a surface to the formation of hybrid bilayer membrane structures, a substrate that will likely be of use in the development of biomimetic sensors. For polymeric interfaces, we have examined free volume and steric limitations imposed on the layered polymer matrix by virtue of the interlayer bonding chemistry used in their construction, and have utilized covalently bound polymer multilayers to demonstrate thermodynamic control over adsorbate-surface interactions. We anticipate that this latter area will prove to be of use in designing surfaces with predetermined selectivity for analytes of interest. The structural tools we have demonstrated allow great latitude in the design of interfacial structures.

Acknowledgement

The authors are grateful to the National Science Foundation (Grant 0090864) and the US Department of Energy (Grant DEFG0299ER15001) for their generous support of this work.

References

[1] P. Kohli, K.K. Taylor, J.J. Harris, G.J. Blanchard, Assembly of covalently-coupled disulfide multilayers on gold, Journal of the American Chemical Society 120 (1998) 11962–11968.
[2] S.B. Bakiamoh, G.J. Blanchard, Demonstration of oriented multilayers through asymmetric metal coordination chemistry, Langmuir 15 (1999) 6379–6385.
[3] J.C. Horne, Y. Huang, G.Y. Liu, G.J. Blanchard, Correspondence between layer morphology and intralayer excitation transport dynamics in zirconium-phosphonate monolayers, Journal of the American Chemical Society 121 (1999) 4419–4426.
[4] J.C. Horne, G.J. Blanchard, Structural mediation of interlayer excitation transport in zirconium phosphonate multilayers, Journal of the American Chemical Society 121 (1999) 4427–4432.
[5] P. Kohli, G.J. Blanchard, Design and growth of robust layered polymer assemblies with molecular thickness control, Langmuir 15 (1999) 1418–1422.
[6] P. Kohli, G.J. Blanchard, Probing interfaces and surface reactions of zirconium phosphate/phosphonate multilayers using 31P NMR spectrometry, Langmuir 16 (2000) 695–701.
[7] P. Kohli, G.J. Blanchard, Applying polymer chemistry to interfaces: layer-by-layer and statistical growth of covalently bound multilayers, in: Polymer Preprints, vol. 41, American Chemical Society, Division of Polymer Chemistry, 2000, pp. 977–978.
[8] P. Kohli, G.J. Blanchard, Applying polymer chemistry to interfaces: layer-by-layer and spontaneous growth of covalently bound multilayers, Langmuir 16 (2000) 4655–4661.
[9] P. Kohli, G.J. Blanchard, Design and demonstration of hybrid multilayer structures: layer-by-layer mixed covalent and ionic interlayer linking chemistry, Langmuir 16 (2000) 8518–8524.
[10] S.B. Bakiamoh, G.J. Blanchard, Surface second harmonic generation from asymmetric multilayer assemblies: gaining insight into layer-dependent order, Langmuir 17 (2001) 3438–3446.
[11] P. Kohli, M.C. Rini, J.S. Major, G.J. Blanchard, Elucidating the balance between metal ion complexation and polymer conformation in maleimide vinyl ether polymer multilayer structures, Journal of Materials Chemistry 11 (2001) 2996–3001.
[12] J.S. Major, G.J. Blanchard, Covalently bound polymer multilayers for efficient metal ion sorption, Langmuir 17 (2001) 1163–1168.
[13] S.B. Bakiamoh, G.J. Blanchard, Characterizing metal phosphonate surface coverage using surface second harmonic generation. Evidence for the coexistence of ordered and disordered domains, Langmuir 18 (2002) 6246–6253.
[14] J.S. Major, G.J. Blanchard, Strategies for covalent multilayer growth: 1. Polymer design and characterization, Chemistry of Materials 14 (2002) 2567–2573.
[15] J.S. Major, G.J. Blanchard, Strategies for covalent multilayer growth: 2. Interlayer linking chemistry, Chemistry of Materials 14 (2002) 2574–2581.
[16] J.S. Major, G.J. Blanchard, Adsorption behavior of polymer-modified interfaces, Langmuir 18 (2002) 6548–6553.

[17] J.S. Major, G.J. Blanchard, Acid-enhanced interfacial polymer layer growth, Chemistry of Materials 14 (2002) 4320–4327.
[18] P. Krysinski, Y. Show, J. Stotter, G.J. Blanchard, Covalent adlayer growth on a diamond thin film surface, Journal of the American Chemical Society 125 (2003) 12726–12728.
[19] P. Krysinski, G.J. Blanchard, Synthesis and characterization of amphiphilic biomimetic assemblies at electrochemically active surfaces, Langmuir 19 (2003) 3875–3882.
[20] J.S. Major, G.J. Blanchard, Achieving thermodynamic control of adsorption and desorption at layered polymer interfaces, Langmuir 19 (2003) 2267–2274.
[21] L. Netzer, J. Sagiv, A new approach to construction of artificial monolayer assemblies, Journal of the American Chemical Society 105 (1983) 674–676.
[22] J. Sagiv, E.E. Polymeropoulos, Adsorbed monolayers. Molecular organization and electrical properties, Berichte der Bunsen-Gesellschaft 82 (1978) 882.
[23] J. Sagiv, Organized monolayers by adsorption: III. Irreversible adsorption and memory effects in skeletonized silane monolayers, Israel Journal of Chemistry 18 (1980) 346–353.
[24] J. Sagiv, Organized monolayers by adsorption: II. Molecular orientation in mixed dye monolayers built on anisotropic polymeric surfaces, Israel Journal of Chemistry 18 (1980) 339–345.
[25] J. Sagiv, Organized monolayers by adsorption: 1. Formation and structure of oleophobic mixed monolayers on solid surfaces, Journal of the American Chemical Society 102 (1980) 92–98.
[26] L. Netzer, R. Iscovici, J. Sagiv, Adsorbed monolayers versus Langmuir–Blodgett monolayers—why and how? II. Characterization of built-up films constructed by stepwise adsorption of individual monolayers, Thin Solid Films 100 (1983) 67–76.
[27] L. Netzer, R. Iscovici, J. Sagiv, Adsorbed monolayers versus Langmuir–Blodgett monolayers—why and how? I. From monolayer to multilayer, by adsorption, Thin Solid Films 99 (1983) 235–241.
[28] R.G. Nuzzo, D.L. Allara, Adsorption of bifunctional organic disulfides on gold surfaces, Journal of the American Chemical Society 105 (1983) 4481–4483.
[29] L.H. Dubois, B.R. Zegarski, R.G. Nuzzo, The chemisorption of organosulfur compounds on gold surfaces—construction of well-defined organic-solids, Journal of Vacuum Science And Technology A, Vacuum, Surfaces, and Films 5 (1987) 634–635.
[30] L.H. Dubois, B.R. Zegarski, R.G. Nuzzo, Fundamental studies of the interactions of adsorbates on organic-surfaces, Proceedings of the National Academy of Sciences of the United States of America 84 (1987) 4739–4742.
[31] R.G. Nuzzo, F.A. Fusco, D.L. Allara, Spontaneously organized molecular assemblies: 3. Preparation and properties of solution adsorbed monolayers of organic disulfides on gold surfaces, Journal of the American Chemical Society 109 (1987) 2358–2368.
[32] R.G. Nuzzo, B.R. Zegarski, L.H. Dubois, Fundamental studies of the chemisorption of organosulfur compounds on Au(111)—implications for molecular self-assembly on gold surfaces, Journal of the American Chemical Society 109 (1987) 733–740.
[33] M.D. Porter, T.B. Bright, D.L. Allara, C.E.D. Chidsey, Spontaneously organized molecular assemblies: 4. Structural characterization of normal-alkyl thiol monolayers on gold by optical ellipsometry, infrared-spectroscopy, and electrochemistry, Journal of the American Chemical Society 109 (1987) 3559–3568.
[34] G.M. Whitesides, E.B. Troughton, C. Bain, S.R. Holmesfarley, S.R. Wasserman, L.H. Strong, Self-assembled organic monolayer films–organic sulfur-compounds on gold and related systems, Journal of the Electrochemical Society 134 (1987) C110.
[35] C.D. Bain, G.M. Whitesides, Molecular-level control over surface order in self-assembled monolayer films of thiols on gold, Science 240 (1988) 62–63.
[36] E.B. Troughton, C.D. Bain, G.M. Whitesides, R.G. Nuzzo, D.L. Allara, M.D. Porter, Monolayer films prepared by the spontaneous self-assembly of symmetrical and unsymmetrical dialkyl sulfides from solution onto gold substrates—structure, properties, and reactivity of constituent functional-groups, Langmuir 4 (1988) 365–385.
[37] A. Ulman, Formation and structure of self-assembled monolayers, Chemical Reviews 96 (1996) 1533–1554.
[38] J.F. Dorsten, J.E. Maslar, P.W. Bohn, Near-surface electronic-structure in Gaas(100) modified with self-assembled monolayers of octadecylthiol, Applied Physics Letters 66 (1995) 1755–1757.
[39] M.J. Lercel, G.F. Redinbo, H.G. Craighead, C.W. Sheen, D.L. Allara, Scanning-tunneling-microscopy based lithography of octadecanethiol on Au and gaas, Applied Physics Letters 65 (1994) 974–976.
[40] O.S. Nakagawa, S. Ashok, C.W. Sheen, J. Martensson, D.L. Allara, Gaas interfaces with octadecyl thiol self-assembled monolayer—structural and electrical-properties, Japanese Journal of Apllied Physics. Part 1, Regular Papers & Short Notes & Review Papers 30 (1991) 3759–3762.
[41] C.W. Sheen, J.X. Shi, J. Martensson, A.N. Parikh, D.L. Allara, A new class of organized self-assembled monolayers—alkane thiols on Gaas(100), Journal of the American Chemical Society 114 (1992) 1514–1515.
[42] H. Lee, L.J. Kepley, H.G. Hong, S. Akhter, T.E. Mallouk, Adsorption of ordered zirconium phosphonate multilayer films on silicon and gold surfaces, Journal of Physical Chemistry 92 (1988) 2597–2601.
[43] H.E. Katz, M.L. Schilling, C.E.D. Chidsey, T.M. Putvinski, R.S. Hutton, Quaterthiophenediphosphonic acid (Qdp)—a rigid, electron-rich building block for zirconium-based multilayers, Chemistry of Materials 3 (1991) 699–703.
[44] H.E. Katz, G. Scheller, T.M. Putvinski, M.L. Schilling, W.L. Wilson, C.E.D. Chidsey, Polar orientation of dyes in robust multilayers by zirconium phosphate–phosphonate interlayers, Science 254 (1991) 1485–1487.
[45] L.A. Vermeulen, J.L. Snover, L.S. Sapochak, M.E. Thompson, Efficient photoinduced charge separation in layered zirconium viologen phosphonate compounds, Journal of the American Chemical Society 115 (1993) 11767–11774.
[46] H.E. Katz, M.L. Schilling, Electrical-properties of multilayers based on zirconium-phosphate phosphonate bonds, Chemistry of Materials 5 (1993) 1162–1166.
[47] M.L. Schilling, H.E. Katz, S.M. Stein, S.F. Shane, W.L. Wilson, S. Buratto, S.B. Ungashe, G.N. Taylor, T.M. Putvinski, C.E.D. Chidsey, Structural studies of zirconium alkylphosphonate monolayers and multilayer assemblies, Langmuir 9 (1993) 2156–2160.
[48] H.E. Katz, Multilayer deposition of novel organophosphonates with zirconium (Iv), Chemistry of Materials 6 (1994) 2227–2232.
[49] J.L. Colon, C.Y. Yang, A. Clearfield, C.R. Martin, Optical investigations of the chemical microenvironment within the layered solid zirconium phosphate sulfophenylphosphonate, Journal of Physical Chemistry 92 (1988) 5777–5781.
[50] L.A. Vermeulen, M.E. Thompson, Stable photoinduced charge separation in layered viologen compounds, Nature 358 (1992) 656–658.
[51] P. Kohli, A.B. Scranton, G.J. Blanchard, Co-polymerization of maleimides and vinyl ethers: a structural study, Macromolecules 31 (1998) 5681–5689.
[52] M.E. Jung, M.A. Lyster, Quantitative dealkylation of alkyl ethers via treatment with trimethylsilyl iodide. A new method for ether hydrolysis, Journal of Organic Chemistry 42 (1977) 3761–3764.
[53] Q. Song, P.W. Bohn, G.J. Blanchard, Radiative dynamics in solution and in molecular assemblies of an h-aggregate-forming stilbazolium amphiphile, Journal of Physical Chemistry B 101 (1997) 8865–8873.
[54] T. Forster, Excitation transfer, Faraday Discussions of the Chemical Society 27 (1959) 300–340.
[55] P. Krysinski, G.J. Blanchard, Synthesis and characterization of amphiphilic biomometic assemblies at electrochemically active surfaces, Langmuir 19 (2003) 3875–3882.
[56] L. Kelepouris, P. Krysinski, G.J. Blanchard, Gauging molecular interactions between substrates and adsorbates. substrate mediation of

surface-bound chromophore vibronic coupling, Journal of Physical Chemistry B 107 (2003) 4100–4106.
[57] I. Willner, E. Katz, Integration of layered redox proteins and conductive supports for bioelectronic applications, Angewandte Chemie. International Edition 39 (2000) 1181–1218.
[58] P. Krysinski, H.T. Tien, A. Ottova, Charge-transfer processes and redox reactions in planar lipid monolayers and bilayers, Biotechnology Progress 15 (1999) 970–990.
[59] D.L. Allara, R.G. Nuzzo, Spontaneously organized molecular assemblies: 2. Quantitative infrared spectroscopic determination of equilibrium structures of solution-adsorbed normal-alkanoic acids on an oxidized aluminum surface, Langmuir 1 (1985) 52–66.
[60] I.C. Stefan, D. Mandler, D.A. Scherson, In situ FTIR-ATR studies of functionalized self-assembled bilayer interactions with metal ions in aqueous solutions, Langmuir 18 (2002) 6976–6980.
[61] R.S. Clegg, J.E. Hutchison, Control of monolayer assembly structure by hydrogen bonding rather than by adsorbate–substrate templating, Journal of the American Chemical Society 121 (1999) 5319–5327.
[62] P.E. Laibinis, G.M. Whitesides, D.L. Allara, Y.T. Tao, A.N. Parikh, R.G. Nuzzo, Comparison of the structures and wetting properties of self-assembled monolayers of normal-alkanethiols on the coinage metal-surfaces, Cu, Ag, Au, Journal of the American Chemical Society 113 (1991) 7152–7167.
[63] P. Krysinski, A. Zebrowska, A. Michota, J. Bukowska, L. Becucci, M.R. Monelli, Tethered mono- and bilayer lipid membranes on Au and Hg, Langmuir 17 (2001) 3852–3857.
[64] S. Gritsch, P. Nollert, F. Jahnig, E. Sackmann, Impedance spectroscopy of porin and gramicidin pores reconstituted into supported lipid bilayers on indium-tin-oxide electrodes, Langmuir 14 (1998) 3118–3125.
[65] H. Hillebrandt, M. Tanaka, Electrochemical characterization of self-assembled alkylsiloxane monolayers on indium-tin oxide (ITO) semiconductor electrodes, Journal of Physical Chemistry B 105 (2001) 4270–4276.
[66] H. Hillebrandt, G. Wiegand, M. Tanaka, E. Sackmann, High electric resistance polymer/lipid composite films on indium-tin-oxide electrodes, Langmuir 15 (1999) 8451–8459.
[67] P. Krysinski, M.R. Moncelli, F. Tadini-Buoninsegni, A voltammetric study of monolayers and bilayers self-assembled on metal electrodes, Electrochimica Acta 45 (2000) 1885–1892.
[68] H.O. Finklea, in: A.J. Bard, I. Rubinstein (Eds.), Electroanalytical Chemistry: A Series of Advances, Marcel Dekker, New York, 1996, pp. 109–335.
[69] A.L. Plant, Supported hybrid bilayer membranes as rugged cell membrane mimics, Langmuir 15 (1999) 5128–5135.
[70] Z. Peng, J. Tang, X. Han, E. Wang, S. Dong, Formation of a supported hybrid bilayer membrane on gold: a sterically enhanced hydrophobic effect, Langmuir 18 (2002) 4834–4839.
[71] V.M. Mirsky, New electroanalytical applications of self-assembled monolayers, Trends in Analytical Chemistry 21 (2002) 439–450.
[72] S.L. Horswell, V. Zamlynny, H.-Q. Li, A.R. Merrill, J. Lipkowski, Electrochemical and PM-IRRAS studies of potential controlled transformations of phospholipid layers on Au(111) electrodes, Faraday Discussions 121 (2002) 405–422.
[73] M. Byloos, H. Al-Maznai, M. Morin, Phase transitions of alkanethiol self-assembled monolayers at an electrified gold surface, Journal of Physical Chemistry B 105 (2001) 5900–5905.
[74] M.H. Schoenfisch, J.E. Pemberton, Effects of electrolyte and potential on the in situ structure of alkanethiol self-assembled monolayers on silver, Langmuir 15 (1999) 509–517.
[75] M.R. Anderson, M. Gatin, Effect of applied potential upon the in situ structure of self-assembled monolayers on gold electrodes, Langmuir 10 (1994) 1638–1641.
[76] B. Raguse, V. Braach-Maksvytis, B.A. Cornell, L.G. King, P.D.J. Osman, R.J. Pace, L. Wieczorek, Tethered lipid bilayer membranes: formation and ionic reservoir characterization, Langmuir 14 (1998) 648–659.
[77] C. Steinem, A. Janshoff, K. von dem Bruch, K. Reihs, J. Goosens, H.J. Galla, Bioelectrochemistry and Bioenergetics 45 (1998) 17.
[78] H. Lang, C. Duschl, H. Vogel, A new class of thiolipids for the attachment of lipid bilayers on gold surfaces, Langmuir 10 (1994) 197–210.
[79] M. Montal, P. Meueller, Proceedings of the National Academy of Sciences 69 (1972) 3651.
[80] M.R. Moncelli, L. Becucci, A. Nelson, R. Guidelli, Electrochemical modeling of electron and proton transfer to ubiquinone-10 in a self-assembled phospholipid monolayer, Biophysical Journal 70 (1996) 2716–2726.
[81] A. Nelson, A. Benton, Phospholipid monolayers at the mercury/water interface, Journal of Electroanalytical Chemistry 202 (1986) 253–270.
[82] L. Zhang, R. Vidu, A.J. Waring, R.I. Lehrer, M.L. Longo, P. Stroeve, Electrochemical and surface properties of solid-supported, mobile phospholipid bilayers on a polyion/alkylthiol layer pair used for detection of antimicrobial peptide insertion, Langmuir 18 (2002) 1318–1331.
[83] P. Krysinski, M. Brzostowska-Smolska, hree-probe voltammetric characterization of octadecanethiol self-assembled monolayer integrity on gold electrodes., Journal of Electroanalytical Chemistry 424 (1997) 61–67.
[84] H. Ron, S. Matlis, I. Rubinstein, Self-assembled monolayers on oxidized metals: 2. Gold surface oxidative pretreatment, monolayer properties, and depression formation, Langmuir 14 (1998) 1116–1121.
[85] I.K. Lednev, T.Q. Ye, L.C. Abbott, R.E. Hester, J.N. Moore, Photoisomerization of a capped azobenzene in solution probed by ultrafast time-resolved electronic absorption spectroscopy, Journal of Physical Chemistry A 102 (1998) 9161–9166.
[86] I.K. Lednev, T.-Q. Ye, P. Matousek, M. Towrie, P. Foggi, F.V.R. Neuwahl, S. Umapathy, R.E. Hester, J.N. Moore, Femtosecond time-resolved UV–visible absorption spectroscopy of *trans*-azobenzene: dependence on excitation wavelength, Chemical Physics Letters 290 (1998) 68–74.
[87] G. Zimmerman, L.Y. Chow, U.J. Paik, The photochemical isomerization of azobenzene, Journal of the American Chemical Society 80 (1958) 3528–3531.
[88] K.H. Drexhage, Influence of a dielectric interface on fluorescence decay time, Journal of Luminescence 1 (2) (1970) 693–701.
[89] W. Lukosz, R.E. Kunz, Fluorescence lifetime of magnetic and electric dipoles near a dielectric interface, Optics Communications 20 (1977) 195–199.
[90] W. Lukosz, R.E. Kunz, Light emission by magnetic and electric dipoles close to a plane interface: I. Total radiated power, Journal of the Optical Society of America 67 (1978) 1607–1619.
[91] C. Girard, O.J.F. Martin, A. Dereux, Molecular lifetime changes induced by nanometer scale optical fields, Physical Review Letters 75 (1995) 3098–3101.
[92] J.J. Macklin, J.K. Trautman, T.D. Harris, L.E. Brus, Imaging and time-resolved spectroscopy of single molecules at an interface, Science 272 (1996) 255–258.
[93] A.A. Blevins, G.J. Blanchard, The effect of positional substitution on the optical response of symmetrically disubstituted azobenzene derivatives, Journal of Physical Chemistry B 108 (2004).
[94] J.A. Dean (Ed.), Lange's Handbook of Chemistry, McGraw-Hill, New York, 1992.
[95] G. Sauerbrey, Zeitschrift für Physik 155 (1959) 206–222.
[96] S. Brunauer, P.H. Emett, E. Teller, Journal of the American Chemical Society 60 (1938) 309.
[97] D.S. Karpovich, G.J. Blanchard, Vapor adsorption onto metal and modified interfaces: evidence for adsorbate penetration of an alkanethiol monolayer on gold, Langmuir 13 (1997) 4031–4037.